Boron-10 nanoparticles filled silicon trenches for thermal neutron detection application

Jia-Woei Wu,[1,a)] Adam Weltz,[2] Machhindra Koirala,[1] James J.-Q. Lu,[1] Rajendra Dahal,[1] Yaron Danon,[2] and Ishwara B. Bhat[1,a)]

[1]Department of Electrical, Computer and Systems Engineering, Rensselaer Polytechnic Institute, 110 8th St, Troy, New York, 12180, USA
[2]Department of Mechanical, Aerospace, and Nuclear Engineering, Rensselaer Polytechnic Institute, 110 8th St, Troy, New York, 12180, USA
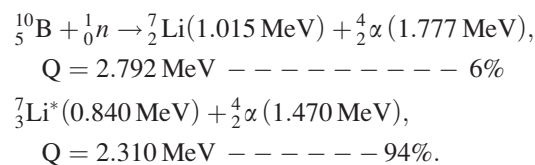
This paper reports on the use of ^{10}B nano/microparticles in order to fill microstructures of deep trenches fabricated in n-type Si (110) bulk wafers for the development of solid-state thermal neutron detectors. The high aspect-ratio trenches were fabricated in the wafer by wet etching, with a trench width of 3.5 to 6 μm and a maximum depth of 120 μm. Boron was diffused at a temperature of $\sim$1000 °C in order to convert the entirety of the delicate Si microstructures into a p^+-n junction diode. The deep trenches of the diode were completely filled with ^{10}B nanoparticles using a simple room-temperature process involving the pumping and venting of a vacuum chamber containing the etched wafer with ^{10}B nanoparticles atop. The simple filling process was reproduced consistently, and the best 2.5×2.5 mm^2 device demonstrated an intrinsic thermal neutron ($E_n < 0.5$ eV) detection efficiency of $32.2 \pm 1.5\%$ under a self-biased condition. This result is promising as it demonstrates a complete, low-cost fabrication process for the development of efficient thermal neutron detectors. *Published by AIP Publishing.* [http://dx.doi.org/10.1063/1.4983289]

Neutron detection is particularly useful for identifying the presence of a special nuclear material (SNM), which is defined as plutonium and uranium enriched in ^{233}U or ^{235}U and is the fissile component of nuclear weapons.[1] ^{3}He proportional counters are widely used for thermal neutron detection because of their high thermal neutron efficiency and insensitivity to gamma rays. Although the shortage of ^{3}He is reportedly not a major problem anymore,[2] the other issues such as bulkiness and high bias voltage (2–3 kV) requirements make ^{3}He detectors impractical for many portable and widespread applications of neutron detection systems for homeland security and other efforts.[3–5] In fact, solid-state thermal neutron detectors have recently been reported as a promising candidate for the replacement of ^{3}He filled detectors for portable applications. Solid-state thermal neutron detectors have the advantages of a negligible microphonic effect, low gamma sensitivity, compact geometry, scalability to larger surface areas, and fast response times. These devices can operate without a bias voltage as long as they are properly designed. Overall, the fabrication, operation, and maintenance costs of solid-state neutron detectors are expected to be significantly lower than those of ^{3}He based detectors.

A heterogeneous solid-state neutron detector is composed of a neutron converter material and reverse biased semiconductor p-n junctions or metal-semiconductor junctions. Common converter materials that have a large thermal neutron capture cross-section are ^{10}B, ^{6}LiF, and ^{157}Gd. These isotopes absorb neutrons based on the ^{10}B(n,α)7Li reaction, the ^{6}Li(n,t)^{4}He reaction, and the ^{157}Gd(n,γ)^{158}Gd reaction, respectively. ^{10}B is selected as the converter material in this work due to its high thermal neutron absorption cross section ($\sim$3840 b at 0.0253 eV, where 1 b = 10^{-24} cm^2) and the compatibility with Si processing. The nuclear reaction of ^{10}B(n,α)7Li is given by[6]

$$^{10}_{5}\text{B} + ^{1}_{0}n \rightarrow ^{7}_{3}\text{Li}(1.015\,\text{MeV}) + ^{4}_{2}\alpha\,(1.777\,\text{MeV}),$$
$$Q = 2.792\,\text{MeV} ------- 6\%$$
$$^{7}_{3}\text{Li}^*(0.840\,\text{MeV}) + ^{4}_{2}\alpha\,(1.470\,\text{MeV}),$$
$$Q = 2.310\,\text{MeV} ------ 94\%.$$

When a thermal neutron interacts with ^{10}B, energetic charged particles, i.e., one alpha (α) particle and one ^{7}Li ion, are produced. The resulting particles can escape the converter material and deposit their energy in the Si junction region, creating electron-hole pairs due to impact ionization. A built-in electric field or an externally applied reverse bias separates the electrons and holes generated in the depletion region or within a diffusion length of the junction, thus producing an electric signal. This signal is sent to an external preamplifier and a shaping amplifier and can be used to identify a neutron event.

A planar solid-state neutron detector consists of a silicon diode with a converter layer coated on the surface. Such detectors have achieved a thermal neutron detection efficiency of only 2%–5%.[7–10] Various designs of neutron detectors that incorporate perforated diode structures are referred to as microstructured solid-state neutron detectors. The microstructured perforations are filled with an aforementioned neutron converter material using various approaches. These microstructured devices with higher intrinsic thermal neutron detection efficiency have been developed by several groups.[11–19]

a)Authors to whom correspondence should be addressed: epyyno1@gmail.com and bhati@rpi.edu

In this paper, several approaches were explored in order to improve the intrinsic thermal neutron detection efficiency and cost-effectiveness associated with fabrication. For example, ion implantation was replaced by a furnace diffusion process in order to reduce the cost and increase the throughput. The cost associated with the fabrication of the deep microstructures was also reduced by replacing deep reactive ion etching (DRIE) with a wet chemical etching process. This wet etching process has the capability to increase the volume of production and has the advantage of less required maintenance costs. Anisotropic chemical etchants—such as potassium hydroxide (KOH) and tetramethylammonium hydroxide (TMAH)—allow for high aspect ratio trenches to be etched into Si (110) wafers. One approach to fill the deep trenches involves low pressure chemical vapor deposition (LPCVD) in order to deposit a boron film using enriched diborane gas (B_2H_6) as a precursor. This method was previously demonstrated by the honeycomb microstructured thermal neutron detectors.[20] However, the CVD boron filling is unreliable for the trench microstructure devices, as the thin Si walls tend to bend and crack when the boron thickness exceeds a few hundredths of a nanometer. This is especially a problem when the trench walls are narrow and deep; unfortunately, deep and narrow trench walls are required to approach the optimal detection efficiency. Further, metal contacts need to be made after the CVD of boron, which requires a top side window in the boron film using a dry etching process. The problems associated with the CVD of boron for trench microstructures were overcome by developing a room temperature boron-filling process for deep trenches ($>100\,\mu m$). This work utilizes commercially available enriched boron nanoparticles (96% [10]B) as a converter material, which replaces the CVD of boron using enriched diborane gas (B_2H_6). The cost of the enriched boron nanoparticles is less than \$48 per gram, while the cost of enriched boron in the form of diborane is about \$2500 per gram. Further, as the boron nanoparticle filling is a room temperature process involving only boron nanoparticles and ethanol, the completion of all diode fabrication steps before the filling process is possible, which simplifies the fabrication process significantly and ultimately lowers the cost of the detector.

A 150 μm-deep, trench microstructured neutron detector filled with 96% enriched boron nanoparticles (with an effective boron density of 0.7 g/cm^3 inside the trench) was simulated using MCNP6.1. The simulation of the device's intrinsic thermal neutron efficiency with variable trench widths (5.0–8.0 μm) and Si wall widths (2.0–4.0 μm) was performed in order to show the efficiency as a function of these parameters, which is shown in Fig. 1(a). The simulations demonstrate that the theoretical maximum efficiency of a 150 μm-deep trench device is ~47.5% with a trench width and a Si wall thickness of 5 μm and 2 μm, respectively. A Si wall width of ~3 μm and a trench width of ~6 μm were chosen in order to ensure the mechanical stability and reproducibility of the overall processes. Moreover, such a wall thickness is thin enough for complete depletion at zero bias due to the continuous p$^+$-n layer formed over the entire walls of the trenches. In this configuration, MCNP6.1 simulations predicted a maximum efficiency of 42% for a trench depth of 150 μm.

A 4-in. (110) n-type Si wafer was used as the starting substrate with a resistivity in the range of 3–10 Ω cm and a wafer thickness of 550 μm. The front side of the wafer was doped with an activated boron source disk (BN-975) at 1000 °C for 30 min in the furnace to form a 0.6 μm-thick p$^+$ layer. The backside of the wafer was doped with POCl$_3$ in the furnace at 950 °C for 30 min in order to obtain a 0.5 μm-thick n$^+$ layer. Photolithography and reactive ion etching (RIE) were used to isolate the devices. A 1.5 μm-thick SiO$_2$ layer was deposited in order to passivate the exposed silicon sidewalls via plasma-enhanced chemical vapor deposition (PECVD). A 200 nm-thick layer of SiO$_2$ was deposited on both sides of the wafer as masking layers for TMAH etching. The SiO$_2$ masking layer was patterned using a parallel trench mask with a 2.5 × 2.5 mm^2 die size, and the trench windows were opened by RIE with a mixture of CHF$_3$ and O$_2$ plasmas. High aspect-ratio trenches with an approximate width of 6 μm and a depth up to 120 μm were etched by 25 wt. % TMAH at 100 °C,[19] which has been optimized with a highest etch ratio of (110) to (111). The continuous p$^+$-n diode formation over the entire trench structure was performed with the boron source disk (BN-975) in the furnace at 1000 °C for 30 min in order to grow a p$^+$ layer that reduces the leakage current and noise level significantly by eliminating the interface traps of the exposed Si after the TMAH etching process. A sputtering system was used for the metal deposition of a 60 nm Ti layer, followed by 300 nm Al as a backside contact for the n$^+$-Si substrate. After the diode fabrication, the remaining major step is the filling of trenches with [10]B nanoparticles.

A room temperature process that simply involves boron nanoparticles and ethanol has been developed for the boron nanoparticle filling. The fabricated device is first covered with the [10]B nanoparticles and placed in a vacuum chamber. The enriched boron nanoparticles were first dispersed in ethanol uniformly in an ultrasonicator. Pumping and venting the vacuum chamber consistently and effectively fills the trenches with the nanoparticles. The chamber was pumped down using a mechanical pump for a few minutes until the ethanol evaporated, resulting in a low pressure inside the trenches. The mechanical pump was then turned off and vented, and so, the pressure of the chamber returned to the atmosphere. The force due to the pressure difference between the inside and outside of the trenches pushed the nanoparticles inside of the trenches.[21] Figure 2 illustrates this simple vacuum-assisted filling process of enriched [10]B nanoparticles into the trenches at room temperature. Finally, front side metallization was performed by sputtering 300 nm of Al using a shadow mask of 1.5 × 1.5 mm^2 window opening. The 4-in. wafer was then diced into individual dies of 1 cm^2 and wire-bonded to a copper plate using silver paint for the following electrical characterization and neutron detection efficiency measurement. Fig. 1(b) shows the schematic of the trench microstructured neutron detector after the enriched nanoparticle filling and metallization.

The quality of the boron nanoparticle filling plays an important role in the efficiency of a neutron detector. Figure 3 shows the cross-sectional SEM images of the filling of enriched boron nanoparticles using the method discussed above. 6 μm-wide and 120 μm-deep trenches were
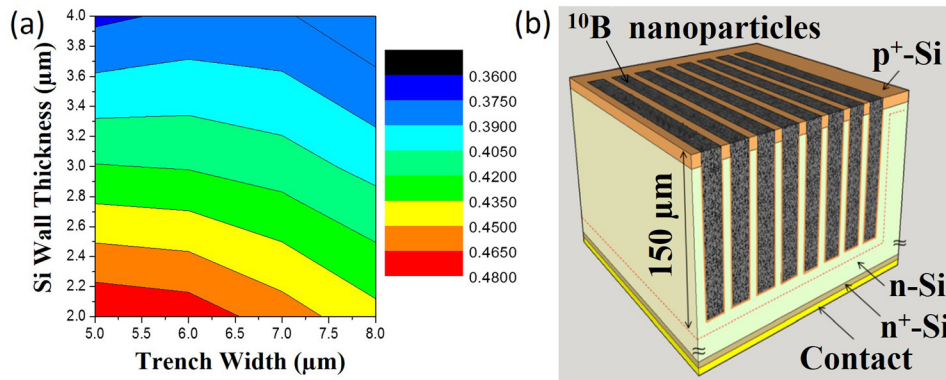
FIG. 1. (a) MCNP6.1 simulation of the intrinsic thermal neutron efficiency of a boron nanoparticle-filled trench detector with a depth of 150 μm, a ^{10}B enrichment of 96%, a nanoparticle filling density of 0.7 g/cm^3, and an LLD of 200 keV. (b) Schematic of a trench-structured neutron detector filled with 96% enriched nanoparticles.

completely filled with the nanoparticles, as shown in Fig. 3(a). This room-temperature vacuum-assisted process for nanoparticle filling into high aspect ratio trenches is simple, effective, and has a very low associated cost. Figure 3(b) also shows the continuous p$^+$-n junction after the boron diffusion process. The effective boron density is another important factor that determines the neutron detection efficiency, which is given by the mass difference of the sample before/after the filling divided by the total volume of the trenches. As observed in Fig. 3(b), the nanoparticles were not closely packed due to irregularity in the shape and size, leading a low effective boron packing density of $\sim$0.7 g/cm^3. Further improvements can be achieved by grinding the particles into smaller sizes and more spherical shapes, which may increase the boron density and improve the detection efficiency.
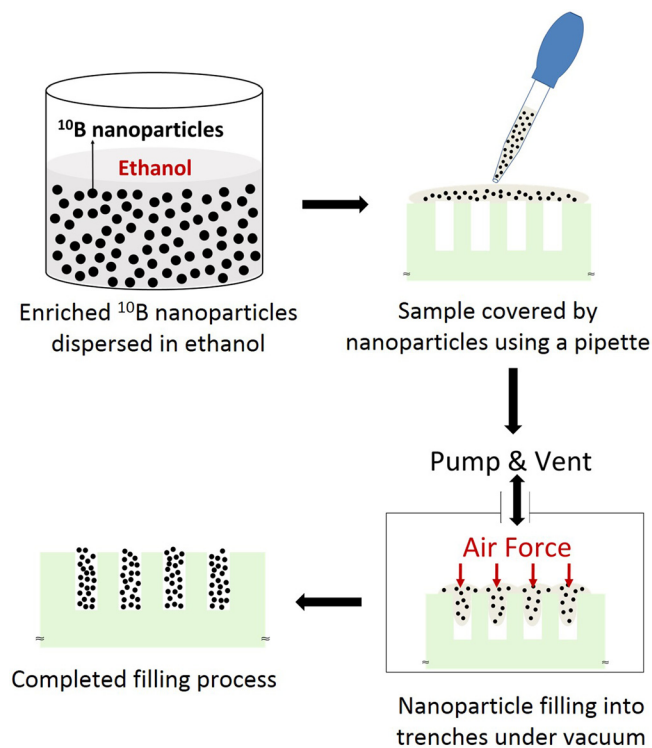

FIG. 2. Schematic illustration of the trench-filling process with enriched ^{10}B nanoparticles by pumping and venting a vacuum chamber. This is a room temperature wet process using a mixture of ^{10}B nanoparticles in ethanol, and so, it can be done as a final step after the front and back metallization of the micro-structured diode completed, which significantly simplifies the fabrication process.

The performance of the micro-structured p$^+$-n diode also contributes to the quality of the neutron detector. A low leakage current (below 1 μA/cm^2) is a key in order to achieve a good signal-to-noise ratio, which also improves the neutron efficiency. In addition, a low leakage current is also required for large-scale applications which involve connecting multiple neutron detectors. Figure 4 shows the current versus the applied bias voltage (I-V) characteristic curve of our 2.5 $\times$ 2.5 mm^2 neutron detector. A low leakage current of 4.8 $\times$ 10^{-8} A/cm^2 at -1 V was achieved due to the formation of the continuous p$^+$-n junction on the surface of trenches. Such a low leakage current leads to a low noise level and is partially responsible for the high reported efficiency. The capacitance of the 2.5 $\times$ 2.5 mm^2 detector is 2 nF at 0 V, which can be directly reduced with the use of higher resistivity wafers for scaling applications. For example, a 2.5 $\times$ 2.5 mm^2 detector with a low capacitance (30 pF) was fabricated using a high resistivity wafer of 5000 Ω cm. This device was successfully scaled to a surface area of 16 cm^2 with minimal loss in efficiency using both series and parallel connections. This scheme will allow for these trench microstructured devices to be scaled to larger areas using such wafers. The combination of this cost-effective and simple process, involving enriched boron nanoparticles and a wet etch process, can contribute to the future development of low-cost, efficient thermal neutron detectors.

The intrinsic thermal neutron efficiency of the devices was measured with a ^{252}Cf spontaneous fission neutron source, which was moderated with high-density polyethylene (HDPE). The HDPE housing has a volume of 61 $\times$ 61 $\times$ 40 cm^3, and the ^{252}Cf source was embedded in the center of the 61 $\times$ 61 cm^2 face, 2.5 cm away from the exposure face of the block. A lightproof Al testing box was used to house the detector, and the detector output was interfaced with a custom-designed preamplifier and a commercial shaping amplifier and Multi-Channel Analyzer (MCA) in order to collect the pulse height spectra.[22] The detector face was aligned vertically with the ^{252}Cf source at a distance of 8 cm from the face of the moderator, as the thermal neutron flux (E$_n$ ≲ 0.5 eV) was previously calibrated at this location using gold and indium foil activation and a highly efficient enriched lithium-glass scintillator. The intrinsic thermal neutron detection efficiency was calculated by recording the count rates for the following measurements: (1) 8 cm away
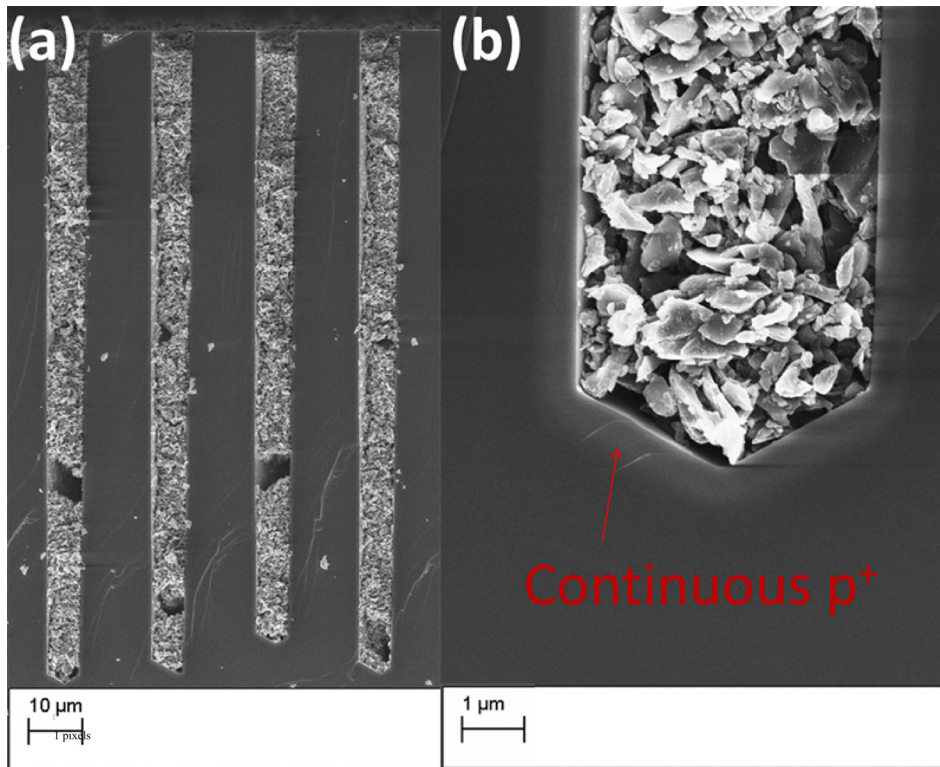
FIG. 3. Cross-sectional SEM images of (a) ~6 μm wide by ~120 μm deep parallel trenches filled with enriched [10]B using the vacuum-assisted process and (b) continuous p$^+$-n formation. The device wafer cleaved after nanoparticle filling to monitor the quality of filling. The effective boron density inside the trench was estimated to be about 0.7 g/cm^3.

from the moderator face, (2) 8 cm away from moderator face covered with 2 mm of Cd, and (3) the corresponding background measurements. Figure 5 shows the pulse height spectrum of each measurement using an ORTEC MCA (model: 927). No detector biasing voltage was applied during these measurements. The intrinsic thermal neutron efficiency of a 2.5×2.5 mm^2 device was measured to be $32.2\% \pm 1.5\%$ with a low-level discriminator (LLD) set to 500 keV, with the calibrated thermal neutron flux of 300 n/cm^2 s at the 8 cm position at the time of the measurements.[18]

In summary, a simple vacuum-assisted process used to fill enriched boron nanoparticles into high aspect-ratio deep trenches fabricated in Si (110) bulk wafers as a neutron converter material for the development of thermal neutron detectors is presented here. The devices were filled with an effective boron density of ~0.7 g/cm^3, and the fabricated 2.5×2.5 mm^2 detector showed an intrinsic thermal neutron detection efficiency of $32.2 \pm 1.5\%$ under self-biased conditions. The discrepancy from the simulated efficiency of 42% by MCNP6.1 could be attributed to the shallower experimental trench depth of 120 μm—compared to a simulated depth of 150 μm. Future work will aim to improve the measured thermal neutron efficiency of the devices by using KOH for trench etching due to its higher etch ratio of (110) to (111) than TMAH. Further improvement in neutron detection efficiency can be achieved by improving the boron nanoparticle density by reducing the average size of the nanoparticles.
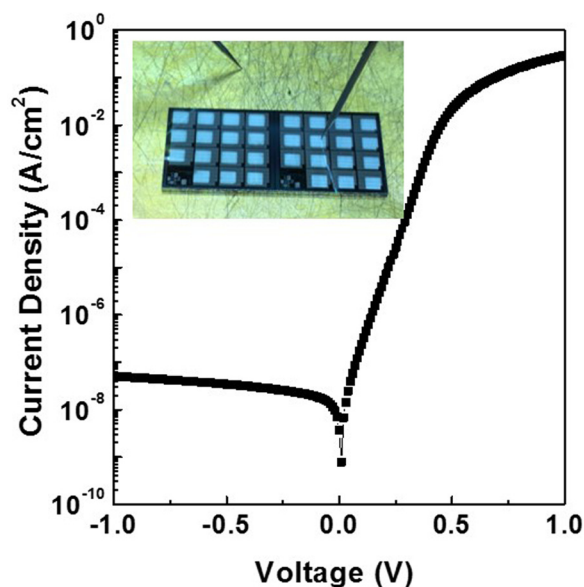

FIG. 4. I-V characteristic of a 2.5×2.5 mm^2 trench-structured neutron detector. A low leakage current density of 4.8×10^{-8} A/cm^2 was obtained at -1 V. The inset shows the optical image of 30 detector dies in a 1 cm $\times$ 2 cm chip.
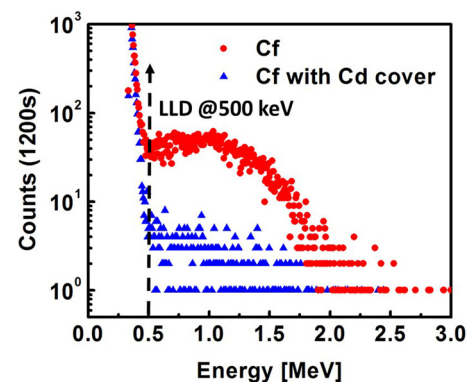

FIG. 5. Pulse height spectra of the trench-structured neutron detector filled with enriched boron nanoparticles with a low level discriminator set to 500 keV.

[1]See http://www.nrc.gov/waste/spent-fuel-transp.html for more information about special nuclear materials; accessed 15 November 2016.

[2]R. Stone, Science **353**, 15 (2016).

[3]T. M. Persons and G. Aloise, *Neutron Detectors Alternatives to Using Heliume-3* (U.S. Government Accountability Office, Washington, DC, 2011).

[4]D. A. Shea and D. Morgan, *The Helium-3 Shortage: Supply, Demand, and Options for Congress* (Congressional Research Service, Washington, DC, 2010).

[5]R. T. Kouzes, J. H. Ely, L. E. Erikson, W. J. Kernan, A. T. Lintereur, E. R. Siciliano, D. L. Stephens, D. C. Stromswold, R. M. Van Ginhoven, and M. L. Woodring, Nucl. Instrum. Methods Phys. Res., Sect. A **623**, 1035 (2010).

[6]G. F. Knoll, in *Radiation Detection and Measurement*, 2nd ed. (John Wiley & Sons, NY, 2010), p. 481.

[7]D. S. McGregor, R. T. Klann, H. K. Gersch, and Y. H. Yang, Nucl. Instrum. Methods Phys. Res., Sect. A **466**, 126–141 (2001).

[8]D. S. McGregor, M. D. Hammig, Y. H. Yang, H. K. Gersch, and R. T. Klann, Nucl. Instrum. Methods Phys. Res., Sect. A **500**, 272 (2003).

[9]P. Chaudhari, A. Singh, A. Topkar, and R. Dusane, Nucl. Instrum. Methods Phys. Res., Sect. A **779**, 33 (2015).

[10]G. Celentano, A. Vannozzi, A. Mancini, A. Santoni, A. Pietropaolo, G. Claps, E. Bemporad, M. Renzelli, F. Murtas, and L. Quintieri, Surf. Coat. Technol. **265**, 160 (2015).

[11]S. L. Bellinger, R. G. Fronk, W. J. McNeil, J. K. Shultis, T. J. Sobering, and D. S. McGregor, Proc. SPIE **7805**, 78050N (2010).

[12]C. M. Henderson, Q. M. Jahan, W. L. Dunn, J. K. Shultis, and D. S. McGregor, Radiat. Phys. Chem. **79**, 144 (2010).

[13]Q. Shao, L. F. Voss, A. M. Conway, R. J. Nikolic, M. A. Dar, and C. L. Cheung, Appl. Phys. Lett. **102**, 063505 (2013).

[14]K.-C. Huang, R. Dahal, J. J.-Q. Lu, Y. Danon, and I. B. Bhat, Appl. Phys. Lett. **102**, 152107 (2013).

[15]K.-C. Huang, R. Dahal, N. LiCausi, J. J.-Q. Lu, Y. Danon, and I. B. Bhat, J. Vac. Sci. Technol. B **30**, 51204 (2012).

[16]D. S. McGregor, S. L. Bellinger, and J. Kenneth Shultis, J. Cryst. Growth **379**, 99 (2013).

[17]R. J. Nikolić, C. L. Cheung, C. E. Reinhardt, and T. F. Wang, *Future of Semiconductor Based Thermal Neutron Detectors* (Barry Chin Li Cheung Publications, CA, 2006).

[18]K.-C. Huang, R. Dahal, J. J. Q. Lu, A. Weltz, Y. Danon, and I. B. Bhat, Nucl. Instrum. Methods Phys. Res., Sect. A **763**, 260 (2014).

[19]J.-W. Wu, K.-C. Huang, A. Weltz, E. English, M. M. Hella, R. Dahal, J. J.-Q. Lu, Y. Danon, and I. B. Bhat, Proc. SPIE **9824**, 982414–982418 (2016).

[20]R. Dahal, K. C. Huang, J. Clinton, N. LiCausi, J.-Q. Lu, Y. Danon, and I. Bhat, Appl. Phys. Lett. **100**, 243507 (2012).

[21]R. K. Trichur, M. Fowler, J. W. McCutcheon, and M. Daily, Inter. Symp. Microelectron. **2010**, 192–195 (2010).

[22]E. English, A. Weltz, R. Dahal, J. J. Q. Lu, Y. Danon, I. B. Bhat, and M. M. Hella, IEEE Trans. Nucl. Sci. **63**, 304 (2016).